Z. Phys. A - Hadrons and Nuclei 343, 267-278 (1992)

Zeitschrift für Physik A Hadrons and Nuclei

Inelastic scattering and nucleon transfer in the system $^{232}Th + ^{206}Pb$ near the Coulomb barrier

G. Eckert[1,*], K. Stelzer[1], R.O. Nelson[1,], Th.W. Elze[1], Th. Happ[1,***], H.J. Wollersheim[2], H. Emling[2], H. Grein[2,†], W. Henning[2], R. Kulessa[2,††], E. Lubkiewicz[2,††], and Ch. Lauterbach[3,†††]**

[1] Institut für Kernphysik, Universität Frankfurt, W-6000 Frankfurt am Main, Federal Republic of Germany
[2] Gesellschaft für Schwerionenforschung, W-6100 Darmstadt, Federal Republic of Germany
[3] Sektion Physik, Ludwig-Maximilians Universität, W-8000 München, Federal Republic of Germany

Received February 10, 1992; revised version March 26, 1992

Nucleon transfer accompanied by Coulomb excitation was studied in the system $^{206}Pb + ^{232}Th$ at $E_{Lab} = 6.4$ MeV/u. Particle-particle-gamma coincidence techniques were used to identify excited states of reaction products populated through inelastic scattering and nucleon transfer reactions. The mean excitation energy was measured by means of a γ-ray energy and multiplicity filter consisting of 6 NaI detectors. Large cross sections for one-neutron and two-neutron pick-up from ^{232}Th are observed. The impact-parameter dependence of the neutron transfer is analyzed in terms of semiclassical barrier penetration models. Using realistic neutron potentials with a diffuse surface, the experimental data are in accordance with the assumption of a "cold" transfer to states near the yrast line.

PACS: 24.10.; 25.70.D + H

1. Introduction

In the present investigation the system $^{232}Th + ^{206}Pb$ was studied at a projectile energy which is approximately 5% above the nominal Coulomb barrier [1]. The main objective of the experiment was to determine the transfer probability of one or two neutrons as a function of the reaction angle, respectively the corresponding distance of closest approach of the colliding nuclei. Based on the measured rate of change of the transfer probability versus the distance of closest approach near the grazing distance, a preceding investigation [2] led to the conclusion that states up to several MeV above the yrast line are populated in the transfer reaction process. Therefore, the present experiment was designed to yield independent information on the excitation energy of the nuclear states to wich the nucleon transfer proceeds by measuring the total emitted γ-ray energy.

In more recent studies of lighter systems, in which reactions of ^{58}Ni and ^{116}Sn projectiles with Dy targets [3, 4] were investigated, similar small radial slopes of the transfer probability were observed. According to those authors the observed behavior in their systems is due to a critical dependence of the slope on the angular momentum to the states excited in the transfer process, rather than to intrinsic excitations of the reaction fragments.

In addition to the transfer probability, the magnitude of the total transfer cross section was of particular interest because in heavy ion transfer reactions instable nuclei can be produced and simultaneously excited by the Coulomb force, thus allowing the study of high-spin states in nuclei which are not accessible to investigations via the usual HI(xn)-reactions.

The experimental method is based on the selection of quasielastic collision processes, by using position sensitive particle detectors in kinematic coincidence, which allow the determination of the scattering angles of the projectile-like and target-like nuclei. For Coulomb trajectories, the scattering angle is uniquely related to the distance of closest approach. The coincident γ radiation, which is characteristic of the Coulomb excitation of either the projectile or the target, or of the products of a nucleon transfer reaction, was measured with high resolution germanium detectors to select the reaction channels. With this technique the cross sections for the different reaction channels can be measured as a function of the distance of closest approach.

In the following section, a brief outline of the experimental particle-γ coincidence procedures is given. The data analysis is described in Sect. 3. In Sects. 4 and 5 experimental results on inelastic scattering and transfer

* *Present address:* Bundeskriminalamt, W-6200 Wiesbaden, Germany
** *Present address:* Los Alamos National Laboratory Los Alamos, N.M. 87545, USA
*** *Present address:* Argonne National Laboratory Argonne, IL 60439, USA
† *Present address:* Hörmann Logistik GmbH, W-8000 München 50, Germany
†† *Present address:* Institute of Physics Jagiellonian University, PL-30-059 Cracow, Poland
††† *Present address:* ESG Elektronik-System Gesellschaft, W-8000 München 80, FRG

reactions are presented. The observed transfer probabilities are examined in the framework of two different barrier penetration models.

2. Experimental methods

The experiment was performed at the UNILAC accelerator of the GSI laboratory at Darmstadt. Targets of 1 mg/cm^2 ^{232}Th were bombarded with ^{206}Pb ions at an incident energy of 6.4 MeV/u, which is slightly above the Coulomb barrier. The reaction products were detected with five position-sensitive parallel-plate avalanche counters. The setup of the detectors in the scattering chamber is illustrated in Fig. 1. Both the recoiling target-like and projectile-like nuclei were detected in coincidence in the array of particle counters. The identities of the nuclei can be distinguished on the basis of kinematic correlations between the scattering angles.

For measurements in the forward direction, a sectioned annular detector was constructed which covers the angular range $15° \leqq \Theta_{\mathrm{Lab}} \leqq 45°$ with respect to the beam at a distance of 12 cm from the target. These angles correspond to values of the closest approach of $15.6 \text{ fm} \leqq D \leqq 34$ fm. Hence, the setup covers overlap parameters $d_{\min} = D/(A_1^{1/3} + A_2^{1/3})$ down to 1.3 fm, where appreciable absorption into more complicated channels is observed. The detector is position-sensitive in both the azimuthal and the polar angles. The azimuthal angle, Φ, is obtained from the anode foil which is divided into 20 radial sections of 18° each. In order to measure the polar angle Θ, the cathode is patterned in concentrical conductor rings, each 1 mm wide, with an insulating gap of 0.5 mm between them. Each ring is connected to its neighbor by a delay-line of 2 ns. The cathode signals are read out from the innermost and outermost rings, and the Θ information is derived from the time difference of the anode and cathode signals. An angular resolution of approximately 1° is obtained.

Double hits within any one Φ section can be eliminated by measuring the sum of the travel times of the signals from the inner and outer rings. This sum coincides with the total delay time of the circuit (160 ns) only for single events.

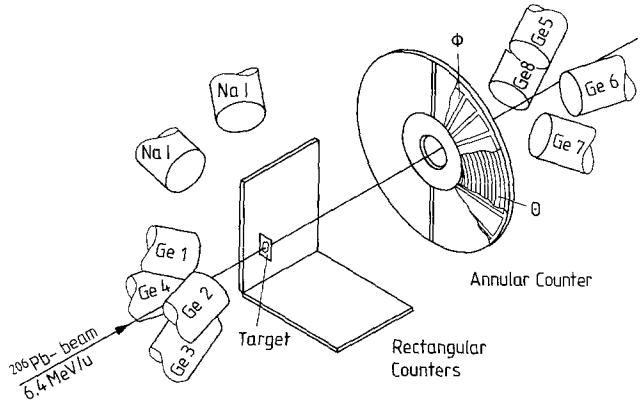

Fig. 1. Experimental set-up for the particle-particle-$\gamma-\gamma$ coincidence measurement of the system ^{206}Pb+^{232}Th. Only two out of four rectangular particle counters are shown

The four rectangular parallel plate counters are used to detect projectile-like or target-like nuclei in coincidence with events in the annular counter. They are placed symmetrically about the beam axis. Each of these rectangular detectors covers an angular range $53° \leqq \Theta_{\mathrm{Lab}} \leqq 90°$ and $\Delta\Phi = 84°$. The detectors were made position sensitive in the Θ direction by using a cathode consisting of a series of nested arcs joined to form a continuous delay line [5]. The cathode was designed with the condition that Θ is constant along each arc. The azimuthal angle is not measured in the rectangular counters, but is determined unambiguously by two-particle kinematics and the location of one particle in the annular counter.

Eight germanium detectors were used to measure the γ radiation. In order to obtain minimum Doppler broadening and the best energy resolution for scattering events around the grazing angle, the detectors were positioned in the direction of the corresponding recoil nuclei at laboratory angles of $\Theta_\gamma = 25°$ (4 detectors), and at 180° to this direction, $\Theta_\gamma = 155°$ (4 detectors).

In addition, 6 large NaI(Tl) detectors of 12.7 cm diameter and 20 cm depth were mounted at $\Theta_\gamma = 90°$ to measure the mean γ energy and the γ multiplicity. The product of these two quantities is used to calculate the total excitation energy after Coulomb excitation or nucleon transfer.

The ^{232}Th target was rotated at an angle of 50° with respect to the beam direction. This angle lies between the largest angle covered by the annular detector (45°) and the smallest angle seen by the rectangular counters (53°). Therefore, shadowing in the target does not affect the particle measurements.

To suppress secondary electrons from the target, a voltage of +20 kV was applied. This measure resulted in a considerable reduction of noise in the particle detectors.

The time and energy signals of all detectors were read out and stored on magnetic tape for the following three trigger conditions: i) particle singles registered in the annular counter, as a measure of the beam intensity, ii) particle-γ coincidences measured with the annular counter and one of the Ge detectors, and iii) particle registered in the annular counter and at least two γ quanta observed in the Ge detectors.

3. Data analysis

3.1. Two-particle kinematics

The kinematic relation between the coincident particles was used to identify projectile-like and target-like nuclei and to define the quasielastic orbits. A two-dimensional plot of the correlation of particle scattering angles is shown in Fig. 2. The abscissa indicates the angle $\Theta_{\mathrm{Lab}1}$ of the particle in the annular counter. The ordinate shows the angle $\Theta_{\mathrm{Lab}2}$ of the coincident particle in the rectangular counter. The two branches correspond to

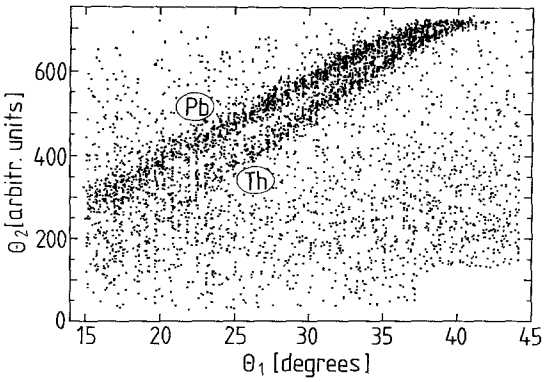

Fig. 2. Measured kinematic relation of the laboratory scattering angles of the projectile-like and recoiling target-like nuclei. Projectiles and recoiling traget nuclei can be scattered into the angular detector at an angle Θ_1. Their identity can be determined from the angle Θ_2 in the rectangular counters

projectiles (Pb-nuclei), respectively recoiling target nuclei (Th) registered in the annular counter.

For the subsequent analysis, in general two-particle events (one particle in annular counter, one particle in the rectangular counters) were selected with the additional condition that the angular correlation of the coincident particles corresponded to that of elastic scattering. The change in the angles in the two-particle correlation caused by Coulomb excitation, or the transfer of a few particles, is smaller than the angular resolution of the particle detectors. In addition, it was required that not more than one particle was registered in the annular counter. With this condition, events with more than two heavy particles, such as fission following inelastic scattering, are eliminated. Events with more than two heavy particles amounted to about 20% of the total yield.

3.2. Characteristic γ radiation

For the analysis of the coincident γ radiation the angular region of the annular detector, $28° \leqq \Theta_{CM} \leqq 150°$, was divided into 10 sections. The corresponding region for the distance of closest approach, $D(\Theta_{CM})$, is $15.6 \leqq D \leqq 33.7$ fm, determined with the well-known relation $D(\Theta) = a_r(1 + 1/\sin(\Theta/2))$, where the quantity a_r is half the distance of closest approach for a head-on collision. In the two windows corresponding to mean distances of closest approach of $D = 17.9$ and 19.7 fm, only one reaction partner is detected by the particle detector array. For these windows the contributions of projectile and target excitation were separated using γ spectra which had been Doppler corrected with an assumed projectile or target motion, respectively. In these spectra, sharp γ lines are produced only for events for which the assumption about the nature of the γ-emitting particle was correct.

Figures 3 and 4 show γ spectra Doppler corrected for the radiation emitted by Th or Pb nuclei. In the upper part of Fig. 3, collisions were selected with an average distance of closest approach of $D = 23.7$ fm. At this

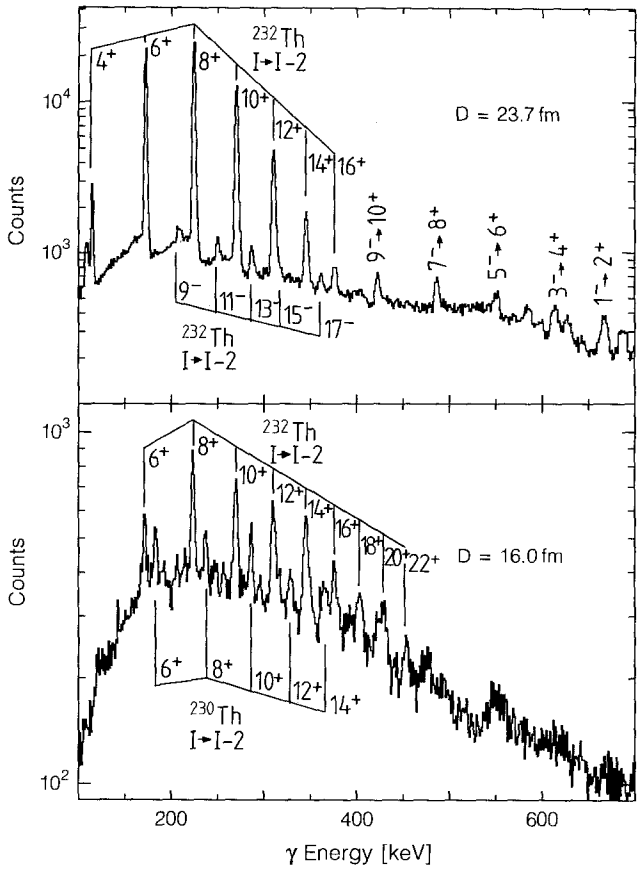

Fig. 3. Ge detector γ-ray spectra Doppler corrected for γ quanta emitted from target-like nuclei. Upper part: distant collision, $D = 23.7$ fm. Lower part: close collision, $D = 16$ fm

distance the excitation is exclusively caused by electromagnetic interaction. The transitions within the ground state and octupole band of ^{232}Th, as well as the interband transitions [6, 7] are observed. The low-energy γ radiation for the transitions $4^+ \to 2^+$ and $2^+ \to 0^+$ in the ground state rotational band were absorbed in the γ detector shields or cut off by the thresholds of the constant fraction discriminators.

The spectrum in the lower part of Fig. 3 was accumulated for the region of the grazing angle with an average distance of closest approach of $D = 16.0$ fm. In this spectrum, the transitions in ^{232}Th are seen up to $22^+ \to 20^+$. For these orbits, the nuclear interaction contributes appreciably. We observe transitions in the ground state band of ^{230}Th up to $14^+ \to 12^+$ ($16^+ \to 14^+$) [6, 8]. These lines are attributed to the transfer of two neutrons from the ^{232}Th nucleus to ^{206}Pb. The corresponding ^{208}Pb reaction partner produced by this transfer process is also observed by its characteristic γ radiation.

To observe the γ rays from ^{208}Pb decay, the Doppler-correction was performed with the assumption that the γ-rays are emitted from projectile-like Pb ions. For the distant collisions in the upper part of Fig. 4, only the lines of the $2^+ \to 0^+$ and $3^- \to 2^+$ transitions in the projectile ^{206}Pb can be identified. In the spectrum for the close collisions in the lower part of Fig. 4, however, the $3^- \to 0^+$ and the $3^- \to 2^+$ transitions in ^{208}Pb are also

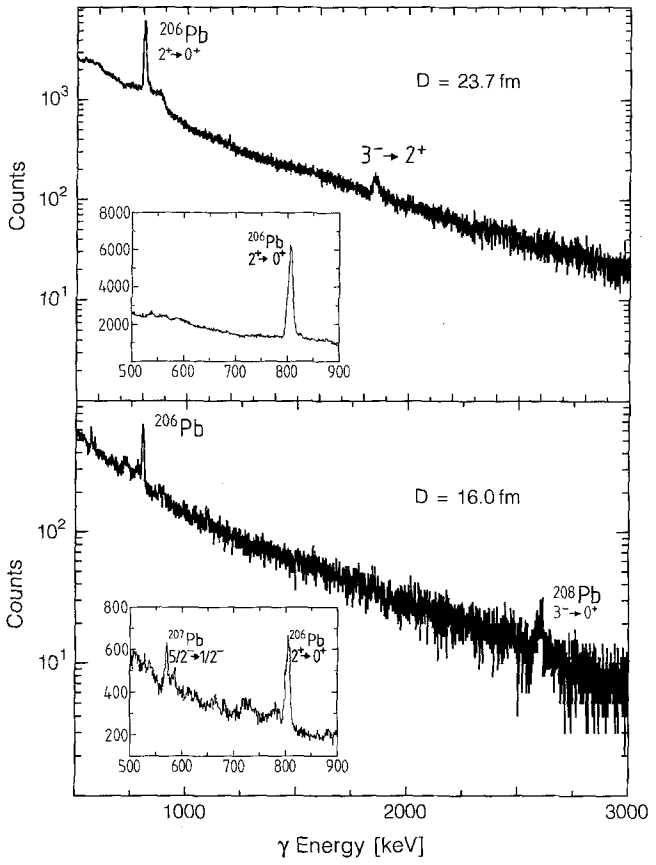

Fig. 4. Ge detector γ-ray spectra Doppler corrected for γ quanta emitted from projectile-like nuclei. Upper part: distant collision, $D=23.7$ fm; lower part: close collision, $D=16$ fm

seen. In addition, the $5/2^- \rightarrow 1/2^-$ transition depopulating the first excited state in ^{207}Pb (see insert) is observed.

The observation of transitions in ^{208}Pb supports the assumption of a two-neutron transfer made on the grounds of the observed lines of ^{230}Th. However, without further information it cannot be excluded that, at least in part, the observed lines of ^{230}Th originate from high excitation of the nucleus ^{231}Th, produced in the one-neutron transfer reaction, followed by the evaporation of a neutron. This reaction channel will be discussed in more detail in Sect. 5.

The $5/2^- \rightarrow 1/2^-$ transition in ^{207}Pb is attributed to the one-neutron transfer from ^{232}Th to ^{206}Pb leading to the system ^{207}Pb+^{231}Th. The analysis of this line was obstructed by the γ background from projectiles hitting the lead collimator of the annular counter. Corresponding γ transitions in ^{231}Th to verify the one-neutron transfer, were not identified in the present experiment. This may be due to the fact that the decay in this nucleus is spread over several paths, each of which is low enough in intensity to escape detection. However, in an earlier investigation of the ^{232}Th−^{206}Pb system at the same bombarding energy [2], we were able to analyze the $5/2^+ \rightarrow 5/2^-$ transition in ^{231}Th. These data have been used to determine the one-neutron transfer probability.

In the present experiment we were able to accumulate for the first time a sufficient number of events to evaluate $\gamma-\gamma$ coincidences for ^{232}Th with high resolution Ge detectors in a particle-particle-$\gamma-\gamma$ experiment. In earlier investigations [7, 9] the ground state transition energies were assigned merely from energy and intensity systematics using particle-particle$-\gamma$ data. The $\gamma-\gamma$ coincidence matrix accumulated from our data verifies the cascade relationship from the $6^+ \rightarrow 4^+$ up to the proposed $26^* \rightarrow 24^+$ transition.

3.3. Average excitation energy

The six NaI(Tl) detectors installed at 90° to the beam were used to determine the average γ-ray energy and the average γ-ray multiplicity. In addition to the selection of two-body events by kinematic conditions on the particles observed, as described above, the γ radiation in the NaI(Tl) detectors was measured in coincidence with the γ lines of ^{232}Th (inelastic excitation) and ^{230}Th (two-neutron transfer) in the Ge detector spectra.

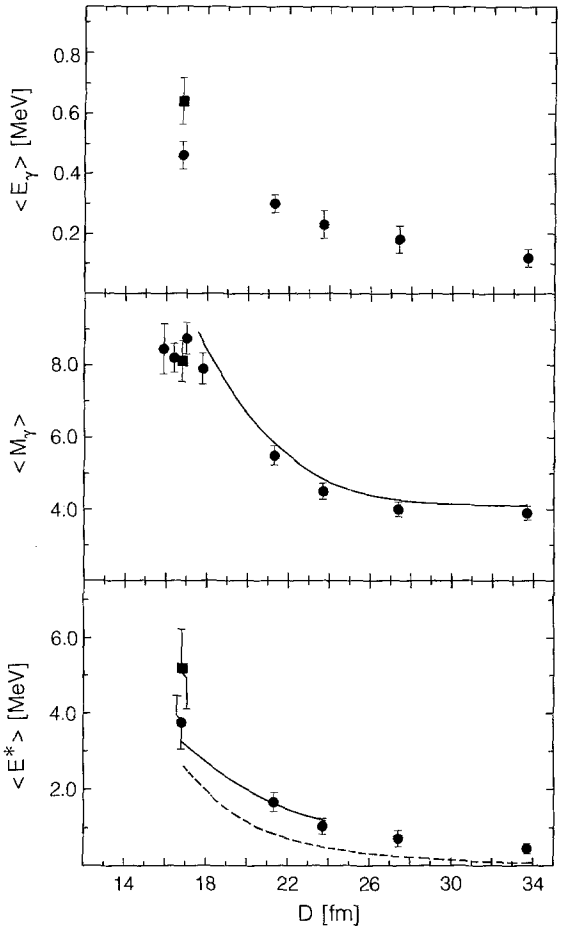

Fig. 5. Experimental and theoretical values for the average γ energy (upper part), γ multiplicity (center part), and excitation energy (lower part). Full dots indicate experimental data for Coulomb excitation of ^{232}Th. The full squares are the data for two-neutron transfer and radiation from ^{230}Th. Dashed lines are calculations for the Coulomb excitation of ^{232}Th; the full curve in the lower parts of the figure includes corrections for the experimental bias towards higher energy γ transitions in the average γ energy

The NaI(Tl) detector energy spectra were analyzed with an unfolding procedure described by Sie [10]. The response matrix for the energy region of 0.2 to 2 MeV was determined with radioactive sources. The average γ-ray energy, $\langle E_\gamma \rangle$, obtained from the unfolding procedure, is shown in the upper part of Fig. 5 as a function of the distance of closest approach, D. The circular symbols describe the data for the excitation of ^{232}Th. These data show a continuous rise with decreasing D. The square symbol summarizes the results for the two-neutron transfer. Because of the low statistics, the transfer data have been summed over the grazing region. As can be seen from Fig. 5, the average γ energy for the transfer events is about 0.15 MeV higher than for Coulomb excitation at the grazing angle. It will be discussed, that the true average γ-ray energy is overestimated by the above procedure because of a low energy cutoff in the experiment. The above arguments concerning the near equivalence of the Coulomb excitation and transfer processes are not invalidated however, because the excitation structure of the isotopes, ^{232}Th and ^{230}Th, is very similar, so that the errors are almost the same in the two cases.

The γ-ray multiplicity was deduced from the experimental data in a procedure described by Hagemann [11], using the relationship

$$\langle M_\gamma \rangle = \frac{\ln(1 - N_C/N_S)}{\ln(1-\Omega)} + 1.$$

The multiplicity depends essentially on the ratio of the coincidence count rate N_C (measured as a $\gamma-\gamma$ coincidence between the Ge and NaI(Tl) detectors) to the singles count rate, N_S, in the Ge detectors. The ratio N_C/N_S was separately determined for Coulomb excitation and two-neutron transfer events by requiring a coincidence with the respective characteristic lines of the two Th isotopes in the Ge detector spectra. The registration probability Ω, the product of the efficiency and the solid angle of the NaI(Tl) detectors, was experimentally determined with radioactive sources. For γ rays from 0.2 to 1.5 MeV it is constant within a few percent. The results of the multiplicity measurement are shown in the center part of Fig. 5. It is seen that the γ multiplicity in the grazing region is the same for Coulomb excitation and two-neutron transfer. The measured multiplicity values for Coulomb excitation are well reproduced by a theoretical calculation (full line in the center of Fig. 5).

The mean excitation energy, $\langle E^* \rangle$, was calculated as the product of the average γ-ray energy times the average γ multiplicity, $\langle E^* \rangle = \langle E_\gamma \rangle \langle M_\gamma \rangle$. The results are shown in the lower part of Fig. 5. The measured mean value of the excitation energy for the two-neutron transfer process is about 1 MeV higher than that for Coulomb excitation. Taking into account the experimental uncertainties one can conclude that Coulomb excitation and two-neutron transfer lead to the same excitation energy within about ± 1 MeV. The dashed line in Fig. 5 is the result of a Coulomb excitation calculation with the assumption that the detector efficiency is independent of the transition energy. Corrections must be applied to account for the lower efficiency below 0.2 MeV in the NaI(Tl) detectors, the strong conversion of low energy transitions, and the coincidence conditions on the Ge detector spectra which favor the registration of higher energy γ-rays in the NaI(Tl) detectors. The full line in Fig. 5 includes all these corrections and is in good agreement with the experimental data for inelastic scattering.

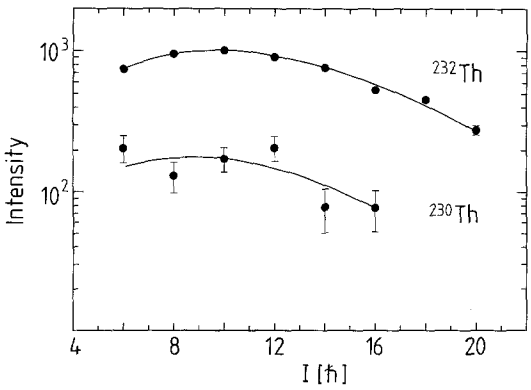

Fig. 6. Measured γ intensities for the transitions in the ground state band of ^{232}Th (inelastic scattering) and ^{230}Th (two neutron transfer)

In the present experiment it was also possible to measure the collective excitation of ^{230}Th, produced by two-neutron transfer, for members of the yrast-band up to high spin. The results for ^{230}Th and for the inelastic excitation of ^{232}Th are shown in Fig. 6 for an angular region around the grazing angle. Although the intensities for ^{230}Th are lower, the relative yield is constant over spin, indicating that both ^{230}Th and ^{232}Th are excited along the yrast line to approximately the same energy. This observation, together with the above results on the experimental mean excitation energy, indicates that there is little intrinsic excitation above the yrast line in ^{230}Th.

4. Inelastic scattering

4.1. Comparison with theoretical cross sections

In our experiment, trajectories with a distance of closest approach between 30 fm and 15,6 fm are selected. We can therefore investigate distant collisions with a purely electromagnetic interaction, and study the onset of the nuclear forces in closer collisions.

For the nucleus ^{232}Th the influence of the nuclear interaction was determined by a comparison of the experimental γ-ray intensities, measured as a function of the distance of closest approach, with the theoretical intensities calculated with a multiple Coulomb excitation program [7, 9]. In a first step, excitation probabilities were calculated as a function of the center-of-mass scattering angle. In this calculation the ground state band and the states of all side bands known [12] were included. For the electromagnetic matrix elements experimentally determined values [9, 13] were used. The ground state band was included up to $I = 34^+$; excitation energies and matrix elements above the experimentally

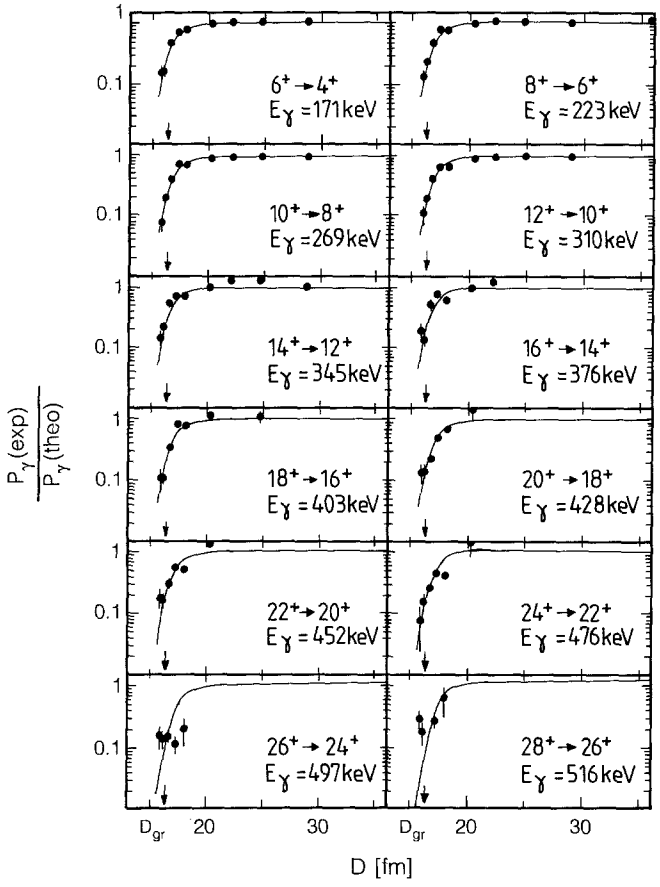

Fig. 7. Ratio of the experimental to theoretical Coulomb excitation for transitions in the ground state band of ^{232}Th as a function of the distance of closest approach. The full lines show the results of a coupled channel calculation (see text). The arrows mark the distance, D_{gr}, for grazing collisions

Table 1. Reaction parameters for the system ^{232}Th + ^{206}Pb

Bombarding energy, E_{Lab} (center of target)	1298 MeV
Center of mass energy, E_{CM}	687 MeV
Wave number, k_∞	60.0 fm^{-1}
Sommerfeld parameter, η	462
Quarter point (grazing) angle	
in the laboratory system, $\Theta_{1/4}$(Lab)	25.6°
in the center of mass system, $\Theta_{1/4}$(CM)	$128.8 \pm \frac{6.0°}{5.2}$
Strong absorption radius, R_{SA}	16.3 ± 0.2 fm
Grazing angular momentum, L_{gr}	222 $\hbar$
Coulomb potential $V_C(R_{SA})$ (Coulomb barrier)	652 MeV
Total reaction cross section, σ_R	870 mb
Neutron transfer cross section	
1n transfer, σ_{1n}	380 ± 40 mb
2n transfer, σ_{2n}	100 ± 10 mb

known level of $I = 28^+$ were extrapolated using rigid rotor relations [14]. In a second step, the γ intensities were calculated taking into account the particle-γ angular correlation, the deorientation of the target nuclei recoiling into vacuum, the finite geometry of the γ detectors, and internal conversion. Coefficients to correct for the deorientation effect were taken from the systematics of Michel et al. [15], and the internal conversion coefficients are from Hager and Seltzer [16]. To correct for the finite geometry, attenuation coefficients of Camp et al. [17] and Barret et al. [18] were used.

The ratios of experimental to theoretical intensities are shown in Fig. 7 for the transitions from $8^+ \to 6^+$ to $28^+ \to 26^+$ as a function of the distance of closest approach D. The ratios were normalized to unity for the transitions from $8^+ \to 6^+$ to $14^+ \to 121$ in the region 20 fm $\leqq D \leqq$ 35 fm, where the interaction is purely electromagnetic. This normalization factor was then used as a common constant for all transitions.

It can be seen that a drastic reduction of the inelastic cross section, caused by the nuclear interaction, sets in at a radial separation between the two ions of 20 fm. As shown in Fig. 7, the reduction of intensity at smaller distances is nearly independent of the transition in the ground state band. The full lines in Fig. 7 represent the results of a coupled channels calculation to be discussed in Sect. 4.2., which includes both the electromagnetic and nuclear interaction. From our data a strong absorption radius and the corresponding center-of-mass grazing angle can be derived with the quarter-point method [19]. The values (indicated by arrows in Fig. 7) are given in Table 1, together with the other reaction parameters for the system ^{232}Th + ^{206}Pb. Our experimental value for the strong absorption radius agrees well with parameterizations by Bass [20] and by Wilcke et al. [21] which are based on an analysis of a number of heavy ion systems: $R_{SA} = 16.2$ fm and $\Theta_{grCM} = 128°$.

4.2. Determination of a nuclear heavy-ion potential

The heavy ion potential acting between the two nuclei can be determined from our measurement of inelastic scattering. The data, shown in Fig. 7, are sensitive to the nuclear potential in the vicinity of the strong absorption radius. Since the inelastic scattering process tests the nuclear potential at large radial values, a proximity type potential $V(s) = V_0 \exp(-s/a)$ has been chosen for the real and imaginary parts of the nuclear potential. The parameters are the distance between the nuclear surfaces (half density radii), s, and the diffuseness of the nuclear surface, a.

The theoretical excitation probabilities for levels in the ground state band of ^{232}Th (full lines in Fig. 7) were calculated with a semiclassical coupled-channels program [22–25] in which the electromagnetic and nuclear interaction are included. While the radius parameters $C_1 = 6.8$ fm and $C_2 = 7.1$ fm were taken from a parameterization of Wilcke et al. [21], the potential depth of the real and imaginary potentials and the diffuseness parameter were varied to obtain the best agreement with the experimentally observed γ intensities as a function of the distance of closest approach.

The best fit parameters of the potential are $V_0 = -45.0 \pm 36.0$ MeV, $W_0 = -30.0 \pm 16.3$ MeV, and $a = 0.76 \pm 0.05$ fm. An equivalent fit to the inelastic scattering data can be obtained with a nuclear potential of the Woods-Saxon form using the same parameters. The large error limits for the depth of the real and imaginary potentials seem to indicate that the results of the calculation are rather insensitive to these values. A more precise statement, based on our optical model parameter searches, is that an almost equally good fit is obtained for any pair of values V_0, W_0, which obeys the approximate empirical relation $W_0 = -(37 + 0.16\, V_0)$ MeV and $-80 \leqq V_0 \leqq -10$ MeV.

This can be understood by the following consideration: When the projectile approaches the strong absorption radius, it starts to interact with the target nucleus through the attractive nuclear force in addition to the Coulomb interaction. The effect of the attractive real nuclear potential, and equally an increase of its value, is to bend the orbit slightly to a closer encounter. Although the change in the orbit is small, because the nuclear potential is small with respect to the Coulomb potential, the higher magnitude of the imaginary potential at the closer distance results in a markedly stronger absorption into non-elastic channels. In order to have the same amount of absorption with an increased real potential, the imaginary potential has to be lowered. For our system, the balance is expressed by the above linear relation between the real and imaginary parts of the potential.

The phenomenological analysis presented in this section allows to include the attractive nuclear interaction in a quantitative determination of the impact-parameter dependence of the scattering angle and the distance of closest approach. Figure 8 shows the classical deflection function for the system $^{232}Th + ^{206}Pb$. The dashed lines in Fig. 8 are the trajectories for pure Coulomb forces, the full lines were calculated by including the attractive nuclear interaction. As a consequence of the small values of the nuclear potential as compared to the Coulomb interaction ($V_C(R_{SA}) = 650$ MeV and $V_N = -2$ to -6 MeV at the strong absorption radius, R_{SA}), the trajectories deviate only slightly from Coulomb orbits. The differences in scattering angle are very small and lie well below the angular resolution of our experiment. The difference in the distance of closest approach is smaller than 0.1 fm except for the closest collisions for which it amounts to about 0.15 fm.

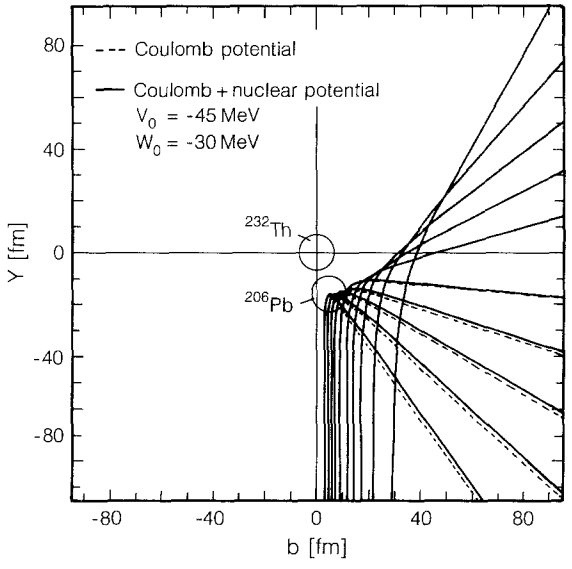

Fig. 8. Trajectories for the system $^{206}Pb + ^{232}Th$ shown for the scattering-angle region of this experiment. Dashed were calculated with a pure Coulomb force, whereas for the full lines the nuclear interaction is included

5. Nucleon transfer

In this section we present the data on one- and two-neutron transfer in the system $^{206}Pb + ^{232}Th$ and discuss the results in the framework or different semiclassical models. Particular interest is dedicated to the question of a "cold" versus a "hot" transfer.

5.1. Q-value window

Transfer reactions between medium and heavy mass nuclei possess a kinematic selectivity with respect to the reaction Q value (Q-value window). In a classical description of the transfer process the optimal Q value is given by the condition that the ingoing and outgoing trajectories join smoothly at the time of transfer. Since in the heavy ion system under consideration, the transfer of a nucleon has only a minor effect on the trajectory, an optimal Q value, Q_{opt}, near zero is expected. For different models, the following values for Q_{opt} for a one-neutron transfer are obtained: -0.21 MeV [26], -0.84 MeV [27] and -0.18 MeV [28]. A comparison of the ground state Q values of Table 2 explains the experimentally observed hindrance of a direct neutron transfer from Pb to Th and the preference of the one and two neutron transfer channels to ^{231}Th and ^{230}Th.

5.2. Neutron evaporation as a competing process

An alternative explanation to populating ^{230}Th by the direct two-neutron transfer is a process in which, in a

Table 2. Ground state Q values for the transfer of neutrons (n) and protons (p) in the system $^{206}Pb + ^{232}Th$

Transfer	Final system	Q value [38] [MeV]
$-1n$	^{231}Th ^{207}Pb	+0.31
$-2n$	^{230}Th ^{208}Pb	+2.55
$+1n$	^{233}Th ^{205}Pb	−3.30
$+2n$	^{234}Th ^{204}Pb	−3.85
$-1p$	^{231}Ac ^{207}Bi	−4.20
$+1p$	^{233}Pa ^{205}Tl	−2.00

first step, a neutron is transferred together with sufficient energy to populate a highly excited state in ^{231}Th. In a second step, this highly excited state then decays by neutron emission to ^{230}Th. The existence of such reaction channels has been considered by several authors, in the case of Th by Gerl [13] and Happ [29].

This contribution can be estimated by measuring the intensity of emitted neutrons in coincidence with the heavy particles. A convenient method is to use the Ge detectors of the experimental set-up, which register neutrons with high efficiency via the $(n, n'\gamma)$ reactions in the germanium isotopes. In our evaluation, the 4 germanium detectors positioned in the forward direction at $\Theta_{Lab}=25°$ were used. In the γ-ray spectra measured for events in which coincidence with more than two particles in the annular counter was registered (thus representing fission and background reactions in carbon and oxygen impurities of the target) the lines from neutron inelastic scattering on ^{70}Ge, ^{72}Ge, and ^{74}Ge were observed with appreciable intensity. Such events however, were not seen in the γ spectra accumulated with the condition of two-particle kinematics and grazing collisions. We can give an upper limit for the contribution of an evaporation process to the production of ^{230}Th by considering the ratio of the detection efficiencies of the Ge detectors for neutrons and γ quanta. The detection efficiency for the neutrons via the $(n, n'\gamma)$ reaction was determined by a Monte Carlo calculation taking into consideration the forward peaking of the neutron distribution due to the high recoil velocity. The calculation shows that our detectors are by a factor of 20 more sensitive to neutrons emitted by ^{231}Th than to γ rays from the same nucleus. The result of the analysis is that less than 5% of the γ lines from ^{230}Th can originate from neutron evaporation of ^{231}Th. Hence, for the system ^{206}Pb+^{232}Th the predominant production process of ^{230}Th is the two-neutron transfer.

5.3. Transfer cross sections

The cross section for one-neutron transfer was determined from the γ spectra of an earlier experiment [2]. A γ-line at 185 keV was assigned to the γ-transition depopulating the band head of the rotation aligned $j_{15/2}$-neutron band in ^{231}Th.

The cross section for the two-neutron transfer was determined from the ratio of the γ intensities of ^{230}Th and ^{232}Th to the cross section for Coulomb excitation in ^{232}Th. In order to collect the whole intensity for the two reaction channels, the transition $8^+ \rightarrow 6^+$ was chosen.

For the Coulomb excitation of ^{232}Th the cross section was calculated as described in Sect. 4.1. This cross section was used to normalize the experimental data in the region $D \geqq 20$ fm for which Coulomb excitation is the only process with measureable strength. In Fig. 9 the cross sections are given relative to the Rutherford scattering cross section, and plotted as a function of the distance of closest approach. The theoretical cross section for Coulomb excitation is shown as curve *a* of Fig. 9.

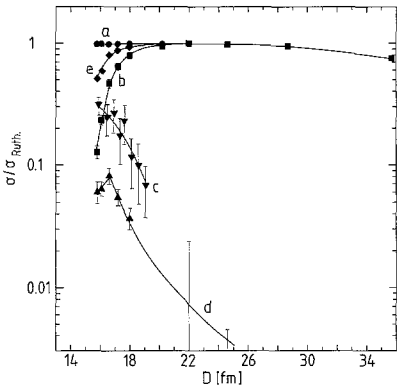

Fig. 9. Cross sections for Coulomb excitation and neutron transfer as a function of the distance of closest approach, D. The cross sections are normalized to the Rutherford scattering cross section. *a* Theoretical cross section for Coulomb excitation. *b* Experimental cross section for Coulomb excitation. *c* Cross section for $1n$ transfer, *d* cross section for $2n$ transfer, *e* sum of b, c, and d

For distances of closest approach of ≈ 20 fm the theoretical cross section is about 99% of the Rutherford cross section. The experimental inelastic scattering cross section, curve *b*, follows the theoretical prediction for Coulomb excitation down to radial distances of about 22 fm. For smaller impact parameters the experimental Coulomb excitation cross section decreases strongly below the theoretical values due to absorption into other channels from the nuclear interaction.

The transfer cross sections are shown by curve *c* for the $1n$ channel and by curve *d* for the $2n$ channel. The cross sections show an almost exponential dependence on the distance of closest approach up to the strong absorption radius. At smaller distances the slope of the cross section for the $1n$ and $1n$ transfer decreases.

It is of interest to consider the sum of the Coulomb excitation and transfer cross sections as shown in curve *e* of Fig. 9. It is seen that the largest part of the flux absorbed from the Coulomb excitation channel is found in the neutron transfer cross sections. Only at distances close to grazing, does additional absorption into other, apparently more complicated reaction channels, set in. It is unlikely that this additional "absorption" can be attributed to an inefficient measurement of the transfer cross sections by our experimental method. It is true that with our method only processes which have led to excited states in the reaction products are detected. However, even if the transfer reaction would proceed to the ground states of the final nuclei, we could expect an appreciable excitation of the reaction product from the strong Coulomb interaction in the outgoing part of the trajectory. A Coulomb excitation calculation shows that in this outgoing part of the orbit still about $12\hbar$ of angular momentum should be transferred in the average.

The total transfer cross sections were determined by integration over the differential cross sections. The cross sections are $\sigma_{1n}=380$ mb for the one-neutron transfer and $\sigma_{2n}=100$ mb for the two-neutron transfer. Together these cross sections amount to more than half of the total reaction cross section (870 mb).

5.4. Transfer probability

Since the trajectories of the collision partners in the present system are essentially Coulomb-like orbits, we define a transfer probability P_{tr} by the following relation between the transfer cross section and the Rutherford cross section [20]

$$\frac{d\sigma_{tr}}{d\Omega} = P_{tr}(1-P_{abs})\frac{d\sigma_{Ruth}}{d\Omega}. \quad (1)$$

In this relation, $(1-P_{abs})$ is the probability that the system escapes absorption into unspecified reaction channels. It should be mentioned here that (1) can be applied even in cases where appreciable absorption takes place [30].

In the evaluation of the experimental transfer probabilities it is important to correctly account for the absorption events [31]. The number of orbits which are available for a transfer reaction, $(1-P_{abs})*(d\sigma/d\Omega)_{Ruth}$, consists of the sum of the elastic scattering, the inelastic excitation, and the transfer processes. Since the nuclei are Coulomb excited essentially with the probability one before they reach the region where neutron transfer takes place, the truly elastic contribution can be neglected. This yields the relation $(1-P_{abs})\cdot(d\sigma/d\Omega)_{Ruth} = (d\sigma/d\Omega)_{CE} + (d\sigma/d\Omega)_{1n} + (d\sigma/d\Omega)_{2n}$. This cross section may be termed "quasi-elastic cross section". It is shown as a function of the distance of closest approach in curve *e* of Fig. 9. With the experimental intensities I_γ^{CE} and I_γ^{tr} for Coulomb excitation and transfer, proportional to the respective cross sections, the experimentally determined transfer probability can be calculated by the simple relation

$$P_{tr,k}^{ex} = \frac{I_\gamma^{tr,k}}{I_\gamma^{CE} + I_\gamma^{tr,1n} + I_\gamma^{tr,2n}}, \quad \text{with } k = 1n, 2n.$$

It should be pointed out that the quantity $(1-P_{abs})$ introduced above is different from the absorption correction made in an earlier paper [2]. In that paper, following a prescription by von Oertzen [30], it was postulated "that in first order the absorption for the transfer channel is the same as that for the inelastic channel".

This procedure did not correctly take into consideration that the removal of flux from the inelastic scattering channel is mainly caused by the transfer process itself. In that case the transfer probability was calculated as $F_{tr} = I^{tr}/I^{CE}$ and was called the "transfer form factor F".

The above relations describe the experimental probabilities, which are effective probabilities P_{eff}. The P_{eff} are identical with the true probabilities, P, if their magnitude is small. If the transfer probabilities are high, however, we have to take into account that neutrons can not only be transferred from ^{232}Th to ^{206}Pb, forming the system ^{231}Th + ^{207}Pb but they can also be transferred back from ^{207}Pb to ^{231}Th forming the original pair of nuclei ^{206}Pb + ^{232}Th. Also higher order transfers become possible, since, based on classical arguments, the relative velocity of the collision partners near the classical turning point of the trajectory is small compared to the Fermi velocity of the neutrons.

If the neutron binding energies for forward and backward transfer are not too different, the effect is approximately accounted for by setting [31–33]

$$P^{ex} = P_{eff} = P - P^2 + P^3 - + \ldots = P/(1+P),$$

where the P^n are the n^{th} powers of P.

The true transfer probability is therefore derived from the γ intensities by $P = P^{ex}/(1-P^{ex})$, i.e. $P_{1n} = I_{1n}^{tr}/(I^{CE} + I_{2n}^{tr})$, and $P_{2n} = I_{2n}^{tr}/(I^{CE} + I_{1n}^{tr})$.

For the case of the $1n$ transfer this result is very close to the relation for the transfer form factor $F = I^{tr}/I^{CE}$, although derived with physically more convincing arguments.

5.5. Comparison with a barrier penetration model with sharp potential boundaries

Experimental transfer probabilities have been compared with predictions of barrier-penetration models [20 and references cited therein]. In the semi-classical model of tunneling, originally developed for sub-Coulomb transfer, i.e., for the case in which the nuclear potentials overlap only weakly, an exponential dependence of the transfer probability with the distance of closest approach is predicted [20] as

$$P_{tr} \sim \sin(\Theta/2)\exp(-2\varkappa D(\Theta)), \quad (2)$$

with $\varkappa = (2\mu B_{eff}/\hbar^2)^{1/2}$, where μ is the reduced mass of the transferred particle and B_{eff} is an effective binding energy of this particle. The basic prediction for sub-Coulomb transfer reactions is therefore an exponential rise of the transfer probability with decreasing distance of closest approach. After an exponential dependence with the distance of closest approach had been established experimentally, the above relation, (2), was applied by several authors [2, 30, 33–35] even to describe reactions at energies above the Coulomb barrier. In particular, it was used to determine the (intrinsic) excitation energy above the yrast line at which the nucleon transfer occurs. This excitation energy can be estimated as $E^* = B_n - B_{eff}$, where B_n is an appropriate mean of the ground state neutron binding energy in the two nuclei of the system. This procedure has been used to distinguish between a "hot" transfer, in which the nucleon is transferred from a intrinsicly excited nucleus ($B_{eff} < B_n$) and a "cold" transfer in which the transfer essentially proceeds from the unheated intrinsic ground state ($B_{eff} = B_n$).

To apply the above relation to our system ^{206}Pb + ^{232}Th, we have determined the true transfer probability P taking into account the absorption as described in Sect. 5.4. The data are shown in Fig. 10 versus the distance of closest approach. The data show an exponential dependence for the $1n$ transfer and an exponential dependence whichs flattens at the grazing distance for the $2n$ transfer. It should be noted that, using (2) the slope for the $2n$ transfer is expected to be about twice the slope of the $1n$ transfer. This holds for a correlated pair transfer and also for a sequential transfer of two neutrons.

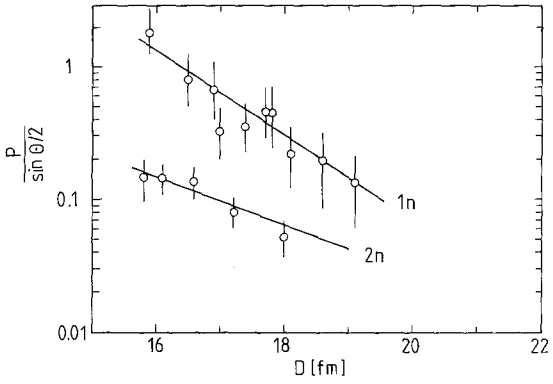

Fig. 10. Probability $P/\sin(\Theta/2)$ for one- and two-neutron transfer as a function of the distance of closest approach, $D(\Theta)$

Table 3. Slope of the transfer probabilities, $K=2\cdot\varkappa$ versus $D(\Theta)$ and effective binding energies B_{eff}

	$1n$ transfer	$2n$ transfer
Experimental slope constant $K=2\cdot\varkappa$ [fm^{-1}]	0.89 ± 0.11	0.41 ± 0.11
Effective binding energy B_{eff} [MeV]	$4.1\ \pm1$	0.43 ± 0.25
Theoretical slope [fm^{-1}]	1.11	2.10
Binding energy B_n [MeV]	6.4	11.6

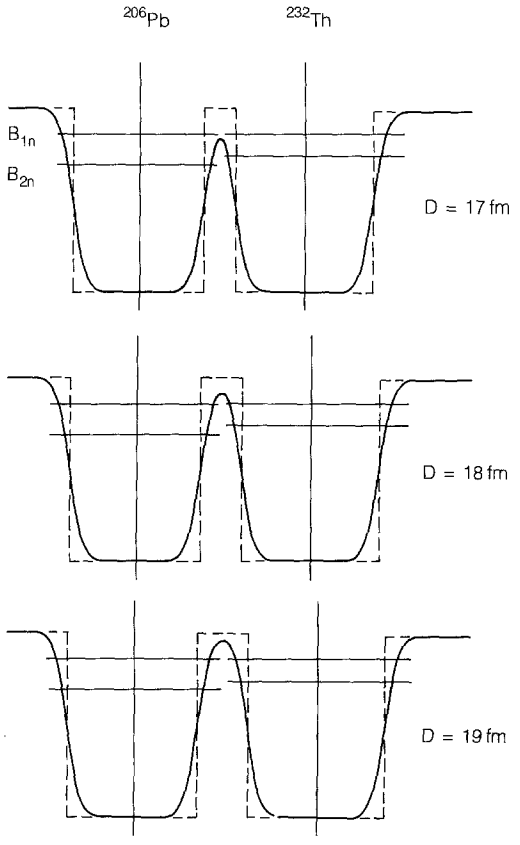

Fig. 11. Neutron potentials for the system ^{206}Pb+^{232}Th for distances of closest approach of $D=17$, 18, and 19 fm

The experimental slope constants, $K=2\varkappa$, the corresponding excitation energies as derived from (2) and the theoretical values for a "cold" transfer are listed in Table 3. From the analysis the $1n$ and $2n$ transfer seem to preferentially populate high lying states, characteristic for a "hot" transfer with excitation energies above the yrast line of 2 MeV ($1n$), and 11 MeV ($2n$).

This interpretation of the transfer probability is in contradiction to our measurement of the excitation energy of ^{230}Th which is the same within 1 MeV as the Coulomb (yrast) excitation of ^{232}Th, indicating a "cold" transfer.

Similar anomalous slope constants were previously reported in [3, 4, 32–34]. In [3, 4] the measured slope was explained by a critical dependence on the angular momenta of the states excited in the transfer process, rather than intrinsic excitations of the collision partners.

For our system, an alternative interpretation will be given in Sect. 5.6. It will be shown that the discrepancies can be removed by a more careful consideration of the shape of the potential barrier for the exchanged neutrons between the colliding nuclei.

5.6. Comparison with a barrier penetration model with diffuse surface of the neutron potential

The transfer probability of (2) is identical to the square of the bound-state wave function of a neutron with binding energy, B_n, outside a square potential with sharp surface. It suggests that the neutron is picked up according to the wave function magnitude with which it exists at a given distance $D(\Theta)$. This relation was also derived by Bass [20] in an optical model treatment of sub-Coulomb transfer, using semi-classical approximations. The common assumption is that the neutron is bound in non-overlapping potentials as shown by the dashed lines in Fig. 11, and that only the tail of the wave function of the transferred neutron enters into the transfer reaction.

An obvious improvement of the barrier penetration model is the use of potentials with a diffuse surface as obtained from an optical model analysis of neutron scattering. We follow Brosa and Gross [36], who first applied these arguments to explain a "neutron rich" mass exchange in heavy systems. The neutron potential of the combined system is taken to be the sum of two potentials of the Woods-Saxon form with parameters taken from the systematics of Bohr and Mottelson [37] for neutron scattering ($V_0=-45$ MeV, and $a=0.67$ fm). To parameterize the nuclear radii, the matter half-density radii, C_i, of our system (Sect. 4.2.) were used. This is equivalent to setting $R_i=r_0 A^{1/3}$ with $r_0=1.15$ fm instead of the value $r_0=1.25$ fm of the global parameter set of Bohr and Mottelson [37]. In Fig. 11 the potentials are shown for our system and distances of closest approach of 17 to 19 fm. The neutron separation energies (^{232}Th: $B_{1n}=6.434$ MeV, $B_{2n}=11.563$ MeV; ^{207}Pb: B_{1n}

$=6.741$ MeV; ^{208}Pb: $B_{2n}=14.109$ MeV [36]) are indicated by horizontal lines. The realistic potentials strongly overlap, and at smaller distances the barrier between the nuclei even drops below the Fermi surface for neutrons in the individual nuclei.

Transfer probabilities were calculated using the parabolic barrier formula of Landau and Lifschitz [39] which is valid also for the case of strong transmission, i.e.

$$P=\left\{1+\exp\left[\frac{2\pi}{\hbar\omega}(V_{\max}+S_n)\right]\right\}^{-1},$$

$$\text{with}\quad \omega=\left(\frac{1}{\mu}\frac{\mathrm{d}^2V}{\mathrm{d}r^2}\right)^{0.5}.$$

Here μ is the reduced mass of the transferred particle, $V_{\max}$ the barrier height and S_n the average neutron separation energy in the nuclei between which the neutron is transferred. As soon as the neutron binding energy approaches the barrier height, the transfer probability goes to unity.

Although this model is still over-simplified, the relative dependence of the transfer probability on the distance of closest approach should be described more realistically. However, one cannot expect to precisely predict the magnitude of the transfer probability because spectroscopic factors and the difference in binding energies are not adequately taken into account.

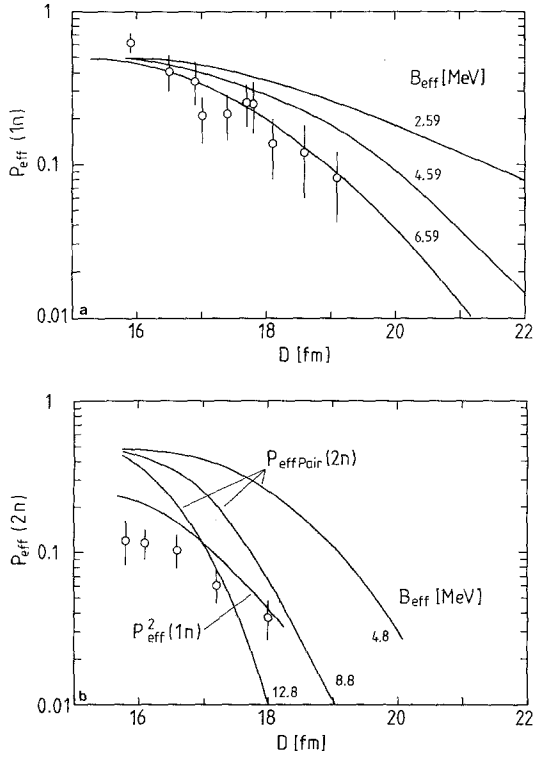

Fig. 12. **a** Comparison of experimental $1n$-transfer probabilities, P_{eff}, with calculations using a diffuse neutron potential and neutron binding energies of 2.59, 4.59, and 6.59 MeV. **b** Comparison of experimental $2n$-transfer probabilities P_{eff} with calculations using a diffuse neutron potential. The full curves are the theoretical results for the correlated pair transfer and effective neutron binding energies of 12.8, 8.8, and 4.8 MeV, and the case of an uncorrelated sequential transfer with a neutron binding energy of 6.59 MeV

In Fig. 12 the experimental transfer probabilities, P_{eff}, are shown for the $1n$ and $2n$ transfer channels versus the distance of closest approach. The $1n$ transfer probabilities (full curves in Fig. 12a) are calculated for 3 values of the neutron binding energy: the average ground state neutron separation energy of 6.59 MeV, and smaller values of 4.59 and 2.59 MeV corresponding to intrinsic excitations of 2 and 4 MeV. The theoretical input parameters were not adjusted to fit the experiment data. This is equivalent to using a spectroscopic factor of unity. The overlap of neutron potentials at distances near the grazing point leads to a constant effective transfer probability, P_{eff}. It should be noted that the asymptotic slope, corresponding to (2), is only reached at distances well over 20 fm. The best agreement between experiment and theory is obtained for the largest neutron binding energy, corresponding to the ground state and "cold" transfer.

For the $2n$ transfer we have to distinguish between the correlated pair transfer, for which the calculation has to be performed with twice the reduced mass of the transferred particle and the corresponding binding energy B_{2n}, which is about twice the value of B_{1n}, and an uncorrelated sequential transfer of two neutrons. In the latter case the effective transfer probability should be given $P_{eff,2n}=P^2_{eff,1n}$.

The two cases are shown by full curves in Fig. 12b, together with the experimental data. For the ^{232}Th $+^{206}$Pb system theoretical values for the correlated pair transfer, calculated with the ground state separation energy and with two separation energies corresponding to 4 and 8 MeV intrinsic excitation, do not describe the experimental values; the dependence of the transfer probability, P_{eff}, on the distance of closest approach, D, is not reproduced. However, there is good agreement with the sequential neutron transfer (lower curve) prediction for a separation energy of 6.6 MeV and if the theoretical values are multiplied with a common factor of 0.5. A "hot" sequential transfer occurring with an appreciably reduced neutron binding energy would show a much flatter dependence with the distance of closest approach and can be excluded.

We conclude that transfer probabilities calculated with diffuse neutron potentials and ground state neutron binding energies agree with the experimental values. From this analysis the $1n$ and $2n$ transfer channels seem to preferentially populate states at or near the yrast line which is in agreement with our measurement of the excitation energy of ^{230}Th.

The authors appreciate the support by H. Folger of the target laboratory of GSI for the target preparation. Thanks are also due to the operating staff of the UNILAC for supplying the heavy-ion beam. One of us (R.O.N.) is indebted to the Alexander von Humboldt-Foundation for a research fellowship. This work was supported by the Bundesministerium für Forschung und Technologie of the Federal Republic of Germany.

References

1. Eckert G.: Ph.D. thesis, University of Frankfurt 1990
2. de Boer F.W.N., Wollersheim H.J., Emling H., Grein H., Grosse E., Spreng W., Eckert G., Elze Th.W., Stelzer K., Lauterbach Ch.: Z. Phys. A – Atomic Nuclei **325**, 457 (1986)
3. Juutinen S., Liu X.T., Sorensen S., Cox B., Kincaid R.W., Bingham C.R., Guidry M.W., Kernan W.J., Wu C.Y., Vogt E., Czosnyka T., Cline D., Halbert M.L., Lee I.Y., Baktash C.: Phys. Lett. B**192**, 307 (1987)
4. Wu C.Y., Liu X.T., Kernan W.J., Cline D., Czosnyka T., Guidry M.W., Kavka A.E., Kincaid R.W., Kotlinski B., Sorensen, S.P., Vogt E.: Phys. Rev. C**39**, 298 (1989)
5. Gruppe A.: Ph.D. thesis, University of Frankfurt 1985
6. Lederer C.M., Shirley V.S.: Table of isotopes. New York: Wiley-Interscience, 1978
7. Ower H., Elze Th.W., Idzko J., Stelzer K., Grosse E., Emling H., Fuchs P., Schwalm D., Wollersheim H.J., Kaffrell N., Trautmann N.: Nucl. Phys. A**388**, 421 (1982)
8. Lauterbach Ch., de Boer J., Mittag Ch., Riess F., Schandera Ch., Briancon Ch., Lefebvre A., Hlavac S., Simon R.S.: Phys. Lett. **140** B, 187 (1984)
9. Ower H.: Ph.D. thesis, University of Frankfurt 1980
10. Sie S.H.: Nucl. Instrum. Methods **155**, 475 (1978)
11. Hagemann G.B., Broda R., Herskind B., Ishihara M., Ogaza S., Ryde H.: Nucl. Phys. A**245**, 166 (1975)
12. Korten W., Gerl J., Ender Ch., Habs D., v. Helmholt U., Heyng H.W., Schwalm D.: Scientific Report MPI Heidelberg 1987
13. Gerl J., Elze Th.W., Ower H., Ronge K., Bohn H., Faestermann T.: Phys. Lett. **120** B, 83 (1983); Gerl J.: Ph.D. thesis, University of Frankfurt 1983
14. Bohr A.: Mat. Fys. Medd. Dan. Vid. Sel. **26**, No. 14 (1952)
15. Michel C., Emling H., Grosse E., Kulessa R., Piercy R., Schwalm D., Seiler-Clark G., Stachel J., Wollersheim H.J.: GSI Scientific Report 1981 (1982)
16. Hager R.S., Seltzer E.C.: Nucl. Data Tables A**4**, 1 (1968)
17. Camp D.C., van Lehn A.L.: Nucl. Instrum. Methods **76**, 192 (1969)
18. Barette J., Lamoureux G., Monaro S.: Nucl. Instrum. Methods **93**, 1 (1971)
19. Blair J.S.: Phys. Rev. **95**, 1218 (1954)
20. Bass R.: Nuclear reactions with heavy ions. Berlin, Heidelberg, New York: Springer 1980
21. Wilcke W.W., Birkelund J.R., Wollersheim H.J., Hoover A.D., Huizenga J.R., Schröder W.U., Tubbs L.E.: At. Data Nucl. Data Tables **25**, 389 (1980)
22. Oberacker V.: Diploma thesis, University of Frankfurt 1973
23. Oberacker V., Holm H., Scheid W.: Phys. Rev. C**10**, 1917 (1974); Oberacker V.: private communication
24. Oberacker V., Soff G.: Z. Naturforschung **32** A, 1465 (1977)
25. Oberacker V., Rhoades-Brown M.J., Satchler G.: Phys. Rev. C**26**, 129 (1982)
26. Toepffer Ch.: Z. Physik **253**, 78 (1972)
27. Brink D.M.: Phys. Lett. **40** B, 37 (1972)
28. Schiffer J.P., Körner H.J., Siemssen R.H., Jones K.W., Schwarzschild A.: Phys. Lett. **44** B (1973); Anantaraman N., Katori K., Schiffer J.P.: Proceedings of the Symposium on Heavy Ion Transfer Reactions, Argonne National Laboratory, Vol. II, 413 (1973)
29. Happ T.: Ph.D. thesis, University of Frankfurt 1988
30. Oertzen W.V., Bohlen H.G., Gebauer B., Künkel R., Pühlhofer F., Schüll D.: Z. Physik A – Atomic Nuclei **326**, 463 (1987)
31. Stelzer K.: Institut für Kernphysik, Universität Frankfurt, Report IKF-52 (1992)
32. Sapotta K.: Ph.D. thesis, University of Frankfurt 1983
33. Sapotta K., Bass R., Hartmann V., Noll H., Renfordt R.E., Stelzer K.: Phys. Rev. C**31**, 1297 (1985)
34. Himmele G., Backe H., Butlar P.A., Habs D., Metag V., Specht H.J., Wilhelmy J.B.: Nucl. Phys. A**404**, 401 (1983)
35. Machiavelli A.O., Deleplanque M.A., Diamond R.M., Stephens F.S., Dines E.L., Draper J.E.: Nucl. Phys. A**432** 436 (1985)
36. Brosa U., Gross D.H.E.: Z. Physik A – Atoms and Nuclei **298**, 91 (1980)
37. Bohr A., Mottelson B.R.: Nuclear structure, Vol. I, p. 236, New York: W.A. Benjamin: 1969
38. Wapstra A.H., Gove N.B.: Nucl. Data Tables A**9** 303 (1971)
39. Landau L.D., Lifshitz E.M.: Quantum mechanics. London: Pergamon Press 1959